

Analysis of the Photothermal Engine Cycle in an AFM-IR Measurement of Photothermal Expansion

Luca Quaroni

Department of Physical Chemistry and Electrochemistry, Faculty of Chemistry, Jagiellonian University, 30-387, Kraków, Poland

e-mail: luca.quaroni@uj.edu.pl

Keywords: Photothermal effect; AFM-IR; micro engine; infrared spectroscopy

Abstract

In the present work we develop a thermodynamic description of signal generation in a micromechanical measurement of the photothermal effect. In the photothermal effect, light absorbed by a material is converted into heat, leading to a local temperature increase and to sample expansion. Photothermal expansion is wavelength dependent and tracks the absorption coefficient of the material, making it a useful probe of the spectroscopic properties of a sample. The local measurement of the expansion can be performed with high spatial resolution by using a micromechanical detection scheme that relies on deflection of a cantilevered probe for atomic force microscopy in contact with the sample. The specific features of this detection mechanism rely on the complex interplay of multiple factors. In the present work we provide a new framework to analyze the factors involved in the detection mechanism, to account for the multiplicity of interactions that may affect the performance of the measurement. We collectively describe the thermomechanical processes that underlie light absorption and photothermal expansion in terms of a thermodynamic engine cycle. We discuss the general properties of this photothermal micromechanical engine, and we derive guidelines for performance optimization of the photothermal measurement. We conclude that the engine is intrinsically inefficient because most or all the energy derived from light absorption is dispersed as heat over one cycle. Nonetheless, we also show that efficiency is not a major consideration when assessed towards the main purpose of this mechanism, which is analytical rather than the conversion of heat into work.

Introduction

Measurement of the photothermal effect allows spectroscopic and imaging experiments over a wide spectral range. Light absorbed by a sample is converted into a temperature increase, leading to sample expansion in a wavelength dependent manner. Among the multiple measurement configurations, the use of atomic force microscopy (AFM) instrumentation to detect photothermal expansion is receiving increasing attention. Such configuration quantifies photothermal expansion by using the deflection of the cantilever of an AFM probe in contact with the sample.[1] Interest in the technique is driven by the promise of endowing conventional infrared spectroscopic analysis with nanoscopic resolution, much better than the optical diffraction limit.[2] The spatial resolution of the measurement does not depend on the wavelength of absorbed light, but on the interplay of tip size and the size of the thermal expansion volume.[3] This is particularly valuable in the extensively used mid-infrared (mid-IR) spectral region, because of the relatively long wavelength ($\lambda \sim 2.5 - 25 \mu\text{m}$), corresponding

to comparable resolution under diffraction limited operation. Delivery on such promise would extend the impact of IR absorption spectroscopy to nanoscale samples, a development of great interest to both academic and industrial researchers. The detection of photothermal expansion with mid-IR light using the deflection of an AFM cantilever was first demonstrated by Anderson using conventional benchtop instrumentation for Fourier-Transform Infrared (FTIR) spectroscopy.[1] While these experiments provided a mechanically-detected interferogram, they did not deliver an absorption spectrum. The method was later developed into a technique for spectroscopic analysis using the pulsed emission from a Free-Electron laser as a light source.[4] The commercial implementation with benchtop laser sources has further widened its appeal and its accessibility to a larger pool of researchers. While the first demonstration of AFM-IR detection was carried out using continuous wave (CW) light sources, the technique is currently implemented mostly with pulsed laser sources. Different names are used to describe the various incarnations of photothermal measurements with AFM detection, of which the most common ones are AFM-IR[4] and Photothermal Induced Resonance (PTIR)[5], the latter normally used in the case of impulsive excitation. In the present work, AFM-IR will be the main moniker, and will be used to cover all implementations of the method.

The technique is currently seeing increased popularity and a general drive towards wider applications in multiple fields, as recently reviewed.[6][7] This apparent success comes at the expense of progress in the investigation of the underlying physical processes. The possibility to relate the absorption spectrum obtained from photothermal measurements to its far-field equivalent relies on having a detailed understanding of the physical processes involved in signal generation and how they relate to the absorption coefficient of the sample. However, some fundamental aspects of the technique remain unclear, and many experimental observations are unexplained by existing theoretical models. The shortcoming arises from the complexity of the micromechanical signal transduction mechanism. It is the purpose of the present analysis to expand the theoretical modelling of such mechanism.

It is already appreciated that the scanning probe detection mechanism introduces a dependence of the signal from the mechanical properties of tip-sample interaction.[8][9][10][11] A less studied aspect is the role of heat-transfer processes on signal generation. This facet has been addressed using Fourier's heat transfer theory,[8][12] but a systematic thermodynamic treatment is still missing. It is the purpose of this work to lay the foundations to model the detection scheme of photothermal expansion based on a micromechanical cantilevered probe. The approach is based on the consideration that, in thermodynamic terms, measurements such as those of an AFM-IR experiment rely on a microscopic engine, a device that converts heat into work. In a micromechanical photothermal measurement, radiation energy heats the sample which by expanding delivers the work necessary to deflect the cantilever of the AFM probe. In the following sections we will assess the merits of this model in describing photothermal experiments with micromechanical detection.

The present analysis will be restricted to the thermomechanical factors that affect the deflection of the cantilever. In a real AFM-IR measurement, other tip-sample interactions can also contribute to deflection and to the overall signal, including optical, photoacoustic,[13] electrostatic[14] and magnetic interactions.[15] While these contributions can be significant, they will not be included in this treatment, which is focused on the component of the signal generated by photothermal expansion.

The analysis will be developed in three main sections. The first section will lay the general concepts in the analysis of a micromechanical photothermal engine. The second section will address the specific case of gradual excitation, whereby the deflecting AFM probe retains contact with the photothermal expansion zone. The third section will discuss the more common case of excitation by a pulsed light source, whereby the rapid expansion and contraction of the sample drives the oscillation of multiple modes of the cantilever. Because of the complexity of impulsive excitation and the multiple interactions involved in the process, beyond simple photothermal displacement, only a qualitative discussion will be provided of the latter.

Results and Discussion

The Micromechanical Detection Scheme of Photothermal Expansion as a Photothermal Engine.

A graphical representation of the micromechanical detection scheme of photothermal expansion is shown in Figure 1, panel A. A cantilevered probe measures light absorption via the expansion of the absorbing region. The sample is mounted as for a conventional AFM experiment and irradiation occurs by focusing light at the tip-sample contact region. An absorbing sample expands upon illumination and the expansion is recorded via the deflection of the cantilever and quantified by the movement of the AFM monitor laser on a four-quadrant detector, as in conventional AFM. The deflection is generally assumed to be proportional to the local absorption coefficient of the sample at the wavelength of irradiation and is used for spectroscopic analysis.[16] Photothermal measurements can be carried out as both spectromicroscopy and imaging experiments. In the former, the probe is kept stationary while the light source is scanned through the spectral range of interest. In the imaging configuration the AFM tip is scanned over the sample while the light source is modulated or pulsed at a single wavelength. A multiplexing approach, whereby a broadband light source excites the sample and is analyzed by a Michelson interferometer is also possible.[1,17,18]

A thermodynamic analysis of the AFM-IR experiment relies on the definition of an engine cycle that best describes the processes occurring during turnover. The first step in the analysis is the ideal breakdown of the measurement into the separate steps or strokes of a cyclic process, as shown in Figure 1, panel B. The sample is the working medium of the engine, and the two terms will be used interchangeably in this work. In contrast to common, macroscopic heat engines, we will consider a solid working medium. The initial state (State 1) is described by a set of thermodynamic variables, pressure (P), volume (V) and temperature (T). In the first stroke, light absorption delivers energy to the sample, simultaneously increasing both T and P, and bringing it to state 2. In the second stroke, the increase in T and P is followed by sample expansion, bringing it to State 3. In the transition from State 2 to State 3, the expansion acts against the force exerted by the cantilever and causes its deflection. In the third stroke, the expanded sample cools down to the initial temperature, typically room temperature, leading to State 4. In the fourth and last stroke, the cooled (thermalized) sample, is compressed back to its initial volume, corresponding to the initial state. In the most general case, the sequence of steps is schematically represented in Figure 1, Panel C, as an ideal cycle in the PV plane (black line). We assume that the engine operates between two temperatures T_1 and T_2 , with $T_1 < T_2$, corresponding to respective heat reservoirs. Under this assumption, the expansion and compression strokes are isothermal transformation, with $T_2 = T_3$ and $T_4 = T_1$. Energy is

absorbed as photons during stroke 1 – 2 and is here represented as an equivalent heat input ($Q_{in} \equiv hv$). The light source formally acts as the high temperature thermostatic reservoir, at temperature T_2 . During stroke 3 – 4, heat is released to the environment (Q_{out}), which acts as the low temperature heat reservoir at temperature T_1 . Expansion work (W_{out}) is executed by the medium on the cantilever during stroke 2 – 3 and is executed by the cantilever on the medium (W_{in}) during compression. As in heat engines, the area of the cycle in Figure 1C provides the total work executed by the engine on the environment ($W_{tot} = W_{out} - W_{in}$). The individual identity of the strokes is a conceptual abstraction, valid for quasi-static transformations, and is lost in a real cycle, which would resemble a distorted ellipsoid (dotted red line).

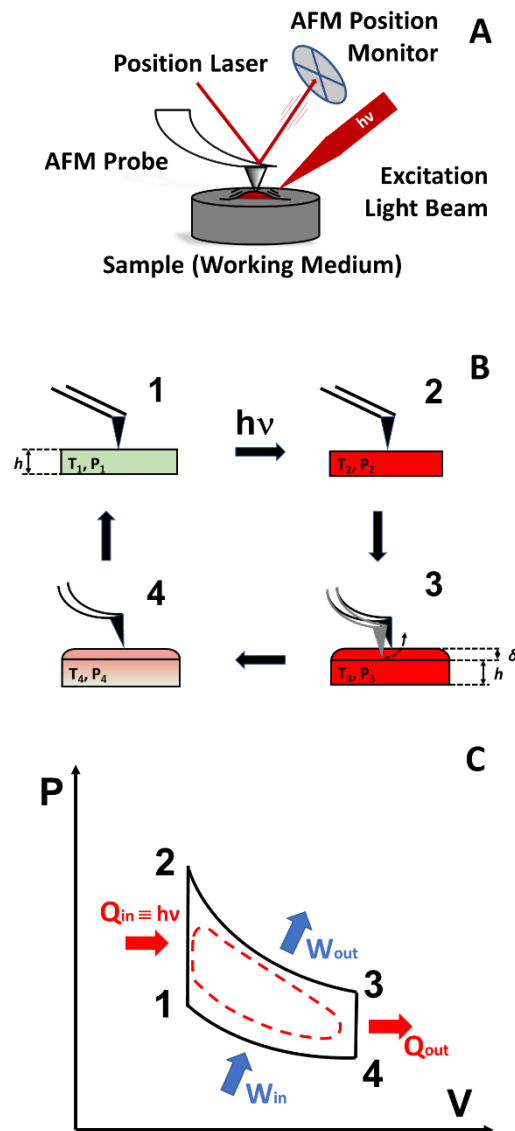


Figure 1. Photothermal signal generation as an engine cycle. **A.** AFM detection of photothermal expansion. **B.** States of the engine and transformations. T_n , P_n , V_n : respectively, temperature, pressure and volume of state n . d sample thickness. u Sample expansion/cantilever deflection. **1.** Initial state. **2.** After temperature increase following light absorption. **3.** After expansion from state 2. **4.** After thermalization of state 3. Red color graphically indicates higher temperature. In the case of isothermal expansion and compression, $T_2 = T_3$ and $T_4 =$

T_1 . In the case of isochoric heating and cooling, $V_1 = V_2$ and $V_3 = V_4$. **C.** The photothermal micromechanical engine cycle. Numbering of cycle states corresponds to the states of Figure 1A. The solid lines represent the quasi-static transformations corresponding to the strokes of the cycle, following the numbering in panel B. The dotted red line represents the overall transformation in the case of a real cycle, where quasi-static conditions are not met.

The cycle of Figure 1C bears resemblance to the working cycle of classical closed-cycle engines operating between two thermal reservoirs at T_1 and T_2 , since the working medium is not exchanged with the environment throughout multiple cycles. The use of a radiation source as the external energy source, in place of heat, qualifies it as a microscopic solar engine. In analogy with mechanical engines, the AFM probe acts as the piston. In contrast to most common heat engines, the medium is a solid and the probe is a spring-loaded piston, with implications that will be discussed later.

The thermodynamic description of Figure 1 allows extracting useful relationships between the thermomechanical properties of the engine and its performance, both in generating the AFM-IR signal and as a micro-optomechanical engine in general. A quantitative description of the system can provide further insight and will be the subject of the following sections. The systems probed by photothermal measurements range from the macroscopic scale, described by classical thermodynamics, to the molecular scale and different theoretical approaches are required to model them. The present analysis will address the workings of macroscale to nanoscale regimes.

As in the analysis of conventional cycles, the cycle represented in Figure 1 assumes quasi-static operation. For finite evolution times, expansion and contraction of the working medium are far from ideal, since cooling of the sample occurs rapidly and continuously during both stages. Heat dissipation takes place at multiple interfaces, including the sample-substrate, sample-tip, and sample-air interfaces, plus any interfaces between sample phases.

The effect of the resulting real PV cycle on performance parameters is graphically represented in Figure 2. Faster heat dissipation under non-thermostatic conditions leads to a smaller area of the cycle. In turn this corresponds to decreased W_{tot} , lower maximum expansion volume of the medium ($V''_{\text{max}} < V'_{\text{max}} < V_{\text{max}}$) and lower deflection ($\delta''_{\text{max}} < \delta'_{\text{max}} < \delta_{\text{max}}$), with a consequently weaker AFM-IR signal.

It is desirable to design the engine cycle to correct for these factors. Optimized thermostatic conditions during expansion and compression, and synchronized heat dissipation at maximum expansion can bring the cycle to be closer to its ideal counterpart, with improved performance, including increased expansion.

The most challenging condition to achieve in a real AFM-IR experiment is the thermostatic stability of the expansion and compression stages. In conventional heat engines, thermostatic conditions are achieved by synchronizing compression and expansion of the working fluid with alternating thermal connection to the temperature reservoirs. This condition is difficult to realize for the AFM-IR engine in Figure 1, because all the thermal connections of the working medium with the surroundings are fixed. The temperature of the sample keeps decreasing during the expansion and compression stages, with a consequent minimization of the isochoric cooling stroke (3-4). As shown in Figure 2, this eventually leads to reduction to a three-stroke cycle, characterized by lower efficiency, reduced expansion, and smaller deflection of the

cantilever. Optimizing the experiment design to approach conditions of thermostatic expansion and compression is a prerequisite for bringing performance closer to the ideal target.

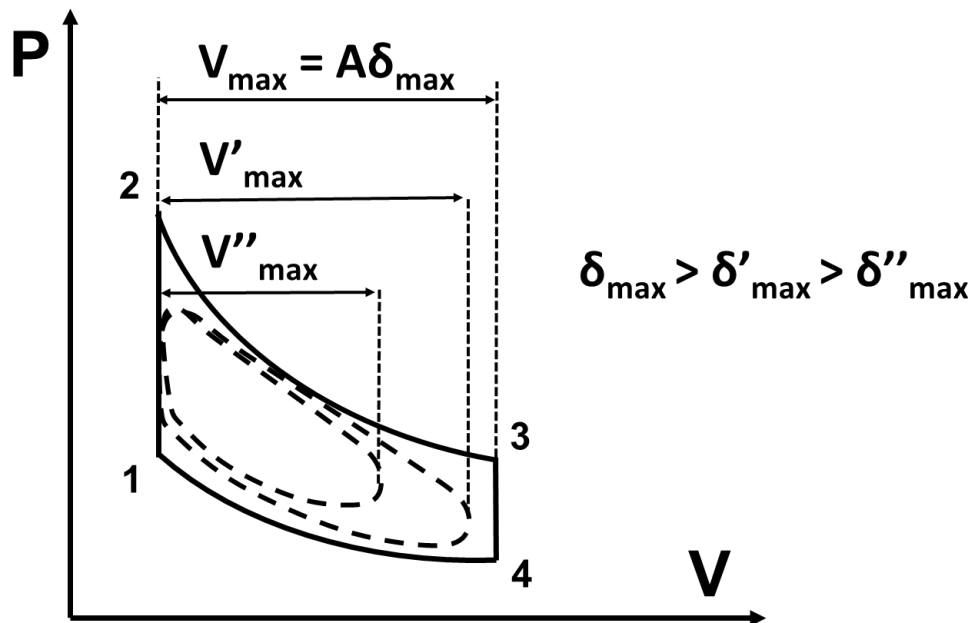


Figure 2. Comparison of ideal and real PV cycles of a photothermal engine. Deviation from the ideal cycle (solid line) is assumed to be mostly from the breakdown of thermostatic conditions during expansion and contraction stages. The resultant cycles (dotted lines) provide reduced expansion, which corresponds to lower maximum expansion volumes ($V''_{\max} < V'_{\max} < V_{\max}$) and reduced deflection of the cantilever ($\delta''_{\max} < \delta'_{\max} < \delta_{\max}$).

Case 1: Spring-Loaded Engine with Gradual Excitation.

One class of AFM-IR experiments involves the use of non-impulsive light sources for photothermal excitation. In such a design, the sample is irradiated with a continuous wave (CW) light source, either a laser or a thermal source. The beam is modulated by chopping at low frequency in the case of a monochromatic laser [1] or, in the case of a broadband beam, it is modulated by scanning the optical path difference of an interferometer.[17,18] This configuration causes a progressive increase of temperature in the medium, until illumination is interrupted, which will be here described as gradual excitation. It is notable that a similar configuration described by Donaldson *et al.*[18] relies on the use of a synchrotron light source. The synchrotron emission is pulsed at such high frequency compared to the response time of conventional infrared detectors that it is generally considered to be a continuous source in optical experiments, although the validity of such assumption has not been confirmed for photothermal experiments.

Under conditions of gradual excitation, heating and expansion occur simultaneously, providing a substantially different and simpler cycle compared to the general one shown in Figure 1. Strokes 1 – 2 and 2 – 3 from Figure 1 can be represented as a single transformation, extending between the two isotherms that represent the thermal reservoirs at T_1 and T_2 (Figure 3, Stroke 1 – 2). Similarly cooling and compression are simultaneous and can be represented as the reverse path in a PV diagram (stroke 2 – 1 in Figure 3).

The harmonic response of the cantilever sets this mechanism apart from that of most conventional heat engines. Work output from the expanding medium (W_{out}) is converted into potential energy by the bending of the cantilever. In an ideal transformation, performed under quasi-static conditions, the tip maintains contact with the sample throughout the cycle. As the medium cools down and contracts, the cantilever completely returns the stored energy as compression work (W_{in}) to the medium. Stroke 2 – 1 is the exact reverse of 1 – 2 and total work output ($W_{tot} = W_{out} - W_{in}$) from the engine is null when the cantilever has returned to its resting position. Such cycle provides zero efficiency and completely negates the usefulness of this mechanism as a heat engine. Despite the fundamental inefficiency, deflection of the cantilever occurs, and an AFM-IR signal can be produced, even in the absence of a net work output. Chopping the light beam at low frequency provides a periodical response of deflection versus time, as schematically shown in Figure 3B. This response was experimentally observed in the first demonstration of the AFM-IR principle. [1]

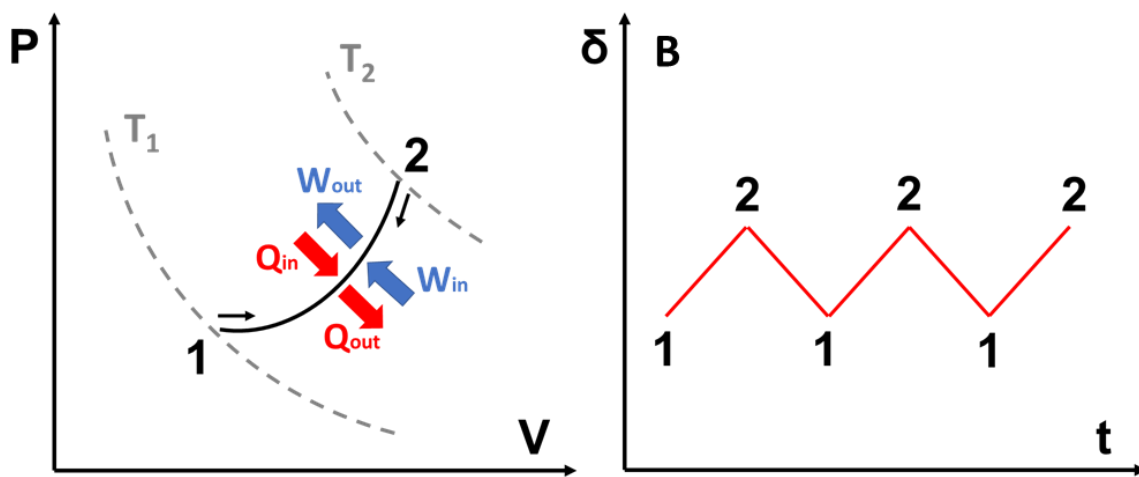


Figure 3. Continuous wave irradiation with a chopped beam. *A. Corresponding engine cycle in a PV diagram. The medium absorbs light, progressing from state 1 to state 2, with a corresponding increase in pressure, volume, and temperature. Interruption of illumination leads to the thermalization and decompression of the sample, returning to state 1 by reversing the expansion stroke. B. Deflection corresponding to the cyclical repetition of the two strokes in panel A.*

A simple treatment, based on the theory of elasticity and the response of a solid to restricted thermal expansion (see Supp. Info.), highlights the main quantities that affect deflection and the AFM-IR signal. In the simplest case, the tip of the probe is approximated by a cylinder providing a flat contact, and the change in temperature is small, so that the change in thermomechanical properties is negligible. The deflection is given by Equation (1).

$$\delta_{max} = (E^*_T \alpha_T \Delta T A)/K \quad (1)$$

E^*_T is the reduced Young modulus for the working medium and tip material at temperature T . α_T is the thermal expansion coefficient of the sample at temperature T , ΔT the temperature difference between the two isotherms ($\Delta T = T_2 - T_1$) and A the contact area between tip and sample.

For the more general case of an axisymmetric tip pressed by an external force against the medium (see Supp. Info.), the formally equivalent Equation 2 applies.

$$\delta_{\max} = E^* \alpha \Delta T \pi r^2 / K \quad (2)$$

πr^2 represents the contact surface of tip and medium and can be expressed as a function of the applied force F_{set} .

$$r^2 = F_{\text{set}}^{2/3} D^{2/3} / (1/R + 1/R')^{2/3} \quad (3)$$

Where $D = \frac{3}{4} ((1-\sigma^2)/E + (1-\sigma'^2)/E')$. σ and σ' are the Poisson ratios for the working medium and the tip respectively. E and E' are the Young modulus of the sample and the tip respectively.

Equations 1 – 3 make explicit the dependence of δ_{\max} from the mechanical properties of the working medium. However, they also imply a dependence from the thermal properties of the medium and the environment. For the same absorbed power, the maximum achievable ΔT depends on thermal contact between the medium and the environment. The availability of channels for rapid thermalization implies lower expansion, lower δ_{\max} and lower AFM-IR signal. Inversely, increased deflection can be ensured by limiting heat transfer between the expanding volume and the environment.

Case 2: Spring-Loaded Engine with Impulsive Excitation.

Impulsive excitation is the most common configuration in contemporary AFM-IR experiments, which rely on laser pulses of duration ranging from less than a nanosecond to ten microseconds to induce a rapid deflection of the cantilever, resulting in a ringdown pattern.[4,19] In this configuration the temperature of the sample increases rapidly, tracking the rise time of the pulse, then decreases exponentially after interruption of the pulse. Because of the timescales involved, it is the least amenable to a description that relies on an equilibrium thermodynamic cycle. Nonetheless, some useful guidelines for the analysis of an impulsive excitation mechanism can be obtained from the cycles of Figure 1 and Figure 2, specifically for the case of a long pulse duration (i.e., the duration of the pulse is non negligible compared to the time required for thermalization). In the case of a long pulse, a rapid increase of the temperature of the sample is followed by an asymptotic convergence to a steady-state temperature (Figure 4A).[20] The rise time of the pulse ensures that most of the temperature increase occurs under isochoric conditions, while expansion occurs under approximately isothermal conditions, corresponding to transformations 1 -2 and 2 -3 of the cycle of Figure 4B. The cycle in Figure 4B can be considered as a limiting case of the cycle in Figure 2, where thermalization occurs together with compression, instead of being a separate transformation. While most of the heating of the medium occurs during the isochoric process 1 – 2, additional heating is performed during the thermostatic expansion 2 - 3.

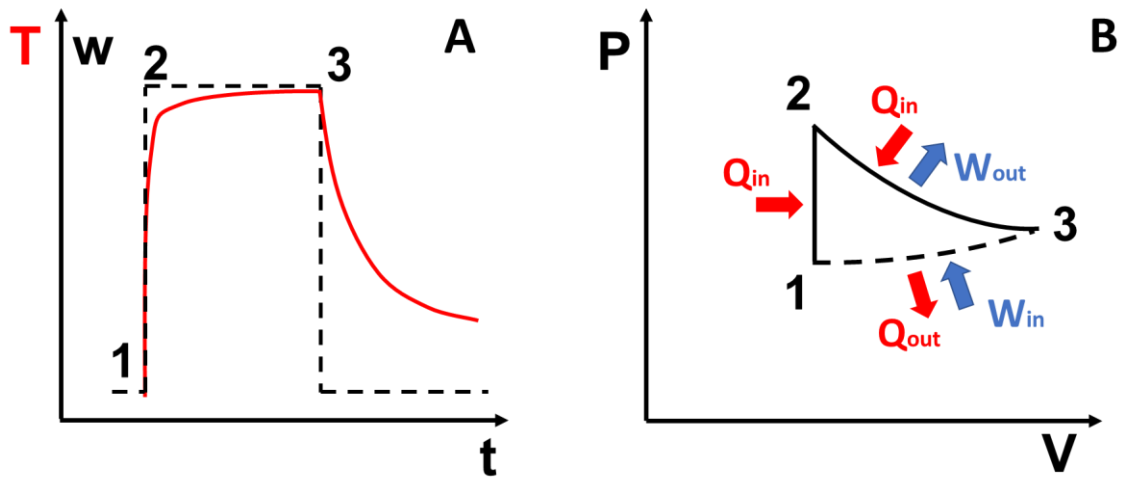


Figure 4. Impulsive excitation and its thermodynamic cycle. **A.** Pulse power (w , dotted line) and temperature increase (T , red line) within the working medium during a pulse. The temperature increases with an exponential behavior during the duration of the pulse, and decreases, also exponentially but at a different rate, after the pulse. **B.** Representation of the process in A in a PV diagram. Rapid sample heating by the pulse corresponds to an isochoric transformation from 1 to 2. Sample expansion during pulse duration corresponds to an isothermal transformation between 2 and 3. Sample contraction during thermalization corresponds to the transformation between 3 and 1.

In contrast to the case of continuous excitation, the cycle in Figure 4B allows in principle for some of the absorbed energy to be converted into work, giving non-zero values of W_{tot} and efficiency. Nonetheless, resulting W_{tot} and efficiency are expected to be small or negligible, limited by the small ΔT produced in AFM-IR experiments, typically in the range of a few or a few tens of degrees Kelvin. As in the case of continuous excitation, the AFM-IR signal increases with the extent of the isothermal expansion stroke and is not directly dependent on W_{tot} .

The possibility for an engine with a spring-loaded piston to produce useful work needs to be addressed. In a conventional heat engine, with a gaseous working medium, expansion increases the potential energy of the spring and compression returns this energy to the medium, providing no net work output. In contrast, the design of the photothermal engine, with a solid working medium, allows the potential energy of the extended spring to be converted into the kinetic energy of an oscillation. This capability can be demonstrated by a *thought experiment* in Figure 4.

In Figure 4A, expansion of the sample brings the cantilever to a deflected position. In contrast to the case of non-impulsive excitation, contact between the probe and the working medium is not retained throughout the cycle. We can think of a situation in which the cantilever is locked in the deflected position by some mechanism that does not consume any energy. While the medium thermalizes and contracts, the cantilever retains the stored potential energy and loses contact with the medium. After thermalization, the retention mechanism is released, and the cantilever is allowed to relax to its equilibrium position. Because of the lack of contact, the cantilever accelerates, as potential energy is converted into kinetic energy, leading to a periodic oscillation. The kinetic energy stored in the oscillation can be converted into usable work by coupling to an external mechanism (not represented here). If the kinetic energy of the oscillation is not recovered, it is dissipated by non-elastic collisions with the sample or by other dissipative processes within the cantilever, leading to various degrees of damping (panels B and C). The latter is the case in an impulsive AFM-IR experiment, in which multiple oscillations of the cantilever are used to extract the AFM-IR signal. Synchronizing the impulse to the frequency of a cantilever oscillation allows resonant energy transfer [9], leading to sinusoidal oscillation at the same frequency as the excitation source (panel D). In the latter case, signal intensity displays a complex dependence from the time structure of the pulses and from the thermal relaxation of the sample, and will not be discussed here. [3]

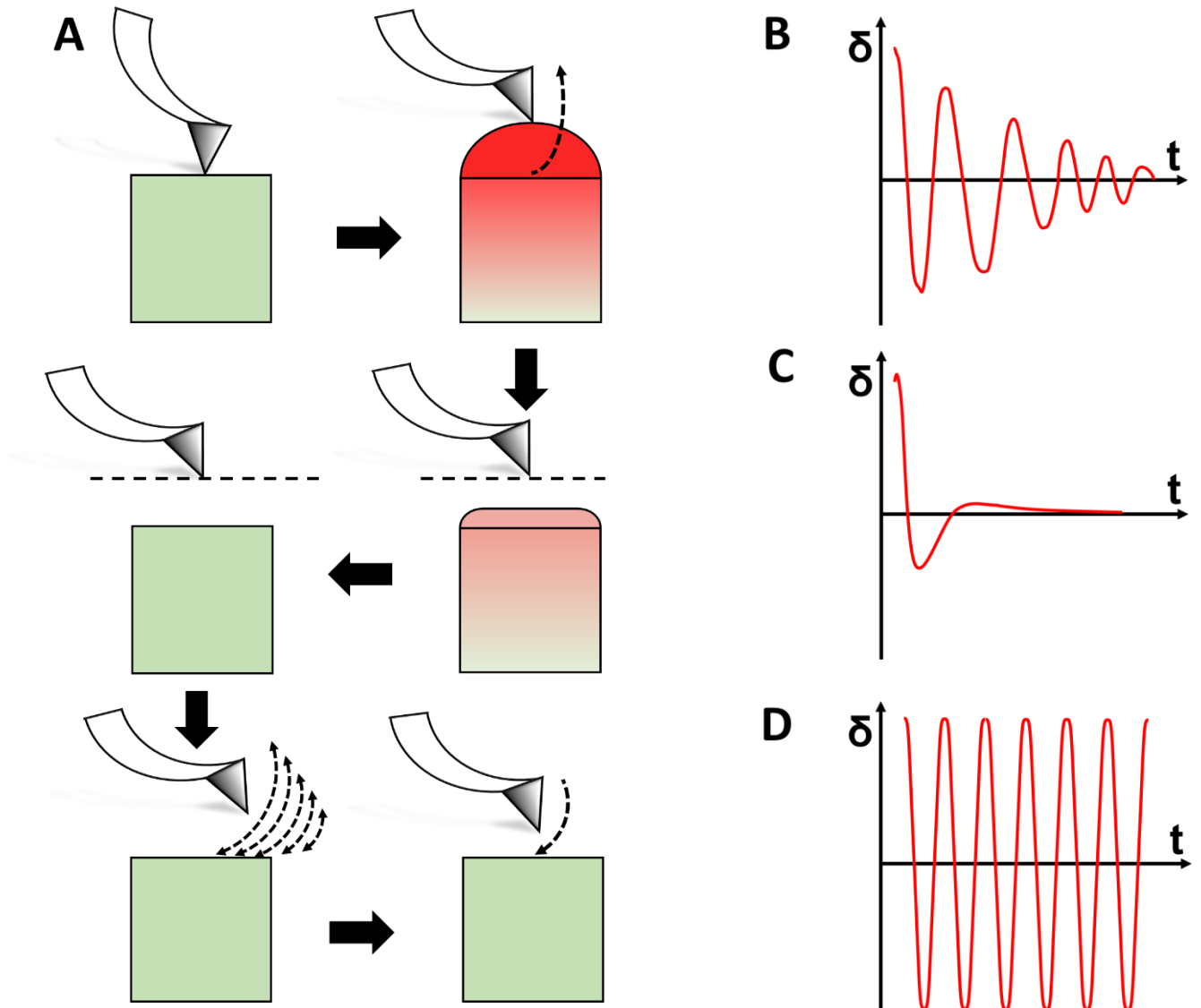


Figure 4. Probe dynamics with impulsive excitation. **A.** Expansion of the medium deflects the cantilever, leading to loss of contact between the two. The medium thermalizes and contracts while the cantilever is retained. Release of the cantilever converts its potential energy into kinetic energy, triggering its oscillation. **B.** Deflection of a lightly damped cantilever oscillation. **C.** Deflection of a highly damped cantilever oscillation. **D.** Deflection of the cantilever in resonant mode operation.

The analysis in Figure 4 relies on the postulate that impulsive excitation leads to loss of contact between the probe and the working medium. It has been previously assumed that in impulsive AFM-IR experiments the probe retains contact with the sample during oscillation and only contact resonances of the cantilever are excited. [8] In contrast, the present discussion argues that conservation of momentum implies that the tip must be displaced from the sample and excitation of non-contact resonance modes of the cantilever must take place following the initial momentum transfer. Excitation of contact resonance modes can develop following energy transfer from non-contact modes, as in the cantilever dynamics in multifrequency AFM experiments. [21]

The AFM-IR signal with impulsive excitation is given by the maximum deflection of the cantilever, δ_{\max} , as in the case of gradual oscillation, or by the intensity of individual resonances in the resonance spectrum of the cantilever. The amplitude of the oscillations (δ_{\max}), and the total energy stored by the cantilever, is a function of the total work performed on the cantilever, in turn dependent on the duration of the pulse. Energy is accumulated in the oscillating cantilever as the combination of potential (U) and kinetic (T) energy of the oscillation. In the case of a harmonic oscillator, this is given by equation 16, where m is the mass of the oscillator (approximated by the point mass of the cantilever/tip system positioned at its center of mass), ω_0 its normal frequency, δ_{\max} the amplitude of the oscillation, and K the force constant.

$$U + T = \frac{1}{2} m \omega_0^2 \delta_{\max}^2 = \frac{1}{2} K \delta_{\max}^2 \quad (16)$$

While equation 16 is the elementary description of energy distribution in a harmonic oscillator, it provides the basic indication that increasing the amount of energy transferred to the oscillator, in the absence of dissipative processes, increases the amplitude of the oscillation. Since the AFM-IR signal is proportional to the amplitude of the oscillation, increased energy transfer corresponds to an increase in the signal. Existing descriptions of energy transfer to an oscillating cantilever have been based on Euler-Bernoulli beam theory and focused on resonant mode operation.[10,11] While they can successfully reproduce the frequency dependence of the transfer function of the cantilever, they cannot account in a quantitative way for the efficiency of energy transfer to the oscillating cantilever, suggesting that additional analysis is required.

The mechanics of impulsive energy transfer to the cantilever are beyond the scope of this discussion, which will instead focus on the thermodynamic arguments of the previous sections. Equation 16 highlights that, in principle, any factors that improve energy transfer to the oscillating cantilever are also expected to increase the amplitude of the AFM-IR signal. Therefore, from a qualitative point of view, some of the same performance factors that maximize δ_{\max} can be identified as for non-impulsive excitation.

One thermodynamic aspect which is particularly relevant to the case of impulsive excitation is the role of the probe as a channel for heat transmission. The possibility for the tip-sample contact surface to act as a channel for thermal relaxation in AFM-IR experiments has been proposed [3], but not systematically investigated. Heat conduction along the AFM cantilever is used in scanning thermal microscopy, [22] and in photothermal cantilever deflection spectroscopy,[23] proving that this is a viable channel for thermal relaxation of the medium. Its contribution is expected to be relevant in the case of thick samples with low thermal conductivity, where the only other channels for thermal relaxation are the sample and the surrounding air. The periodical tip-sample contact can define the duration of thermostatic expansion stages, by allowing rapid heat transfer from the sample at defined time points. In cases where the laser pulse induces direct heating of the cantilever, the contact may also act as a timed heat source towards the sample, modulating its relaxation.[24] Synchronization of the contact with excitation pulses can provide increased deflection by allowing a longer thermostatic expansion stroke. This condition has indeed been realized in a micromechanical heat engine with a periodical cantilevered contact to a heat source and heat sink.[25] In this context, resonant operation provides fine synchronization of laser pulses with the cantilever oscillation, thus providing optimal conditions for heat exchange between the sample and the tip. The timing of excitation and heat relaxation may be a contributing factor to the signal

observed in resonant mode excitation and to the dependence of the resonant signal from the frequency and pulse length of the laser, delivering stronger signal with longer pulses.[3] In agreement with the present analysis, it has been shown by Lu *et al.* that resonant operation provides thermostatic conditions in the measurement of thin films.[26]

Testing the Photothermal Engine Model: Non-Impulsive Excitation

Testing the predictive capability of the photothermal engine model goes hand in hand with its use in the optimization of an AFM-IR experiment. The treatment provided by equations 1 - 3 is limited to the case of excitation by a CW light source, as described by Figure 3. Therefore, the discussion in this section is mostly limited to this specific case. It relies on the consideration that the intensity of the AFM-IR signal parallels the deflection of the cantilever, δ_{\max} .

It follows immediately from equations 1 - 3 that δ_{\max} increases with ΔT and with the optical parameters that affect ΔT , such as the absorption coefficient at the wavelength of excitation. This is the generally accepted dependence of the AFM-IR signal from the macroscopic absorption spectrum of the sample, which is the basis of the spectroscopic and analytical applications of the technique. Equations 1 - 3 also define the dependence of the signal from the thermomechanical properties of the system. Stiffer materials, with larger values of E , deliver stronger signal, although the gain may be counterbalanced by the decrease in α often displayed by the same materials. The deflection also decreases with increasing K , showing that softer cantilevers provide higher sensitivity. Some of these conclusions are known from and in agreement with the analysis by Lu *et al.* [26], while the dependence from K is opposite to the one predicted by Dazzi *et al.* [8]

Equations 1 - 3 also highlight a proportional relationship between the AFM-IR signal and the contact surface between tip and sample. This bears some analogy to the role of the compression ratio on the performance of internal combustion engines. The effect of the tip-sample contact area may be contributing to the difference in signal intensity when measuring convex and concave sample surfaces.[27] While Equations 2 and 3 were derived for two specific geometries, the power dependence between contact surface and force is the same for any geometry, [28] and the proportionality between δ_{\max} and contact area will be retained for any sample and tip geometry. Accordingly, it is expected to be a general conclusion that a better match between tip and sample shape can extend the contact surface and improve the AFM-IR signal.

While the tip-sample contact geometry is well known to affect contact micromechanics in AFM applications, it has received little attention in AFM-IR applications. Existing theoretical treatments of AFM-IR either neglect the role of tip-sample contact [12] or limit the discussion to the effect of the contact on the resonant frequency of the cantilever.[10][11][8] Only the analysis by Dazzi *et al.* and the work by Lu *et al.* explicitly consider the dependence of the force from the contact surface, although the former provides a lower dimensional dependence.[8][26] The present treatment confirms that increasing the contact surface delivers a proportionally higher force and deflection, thus increasing the AFM-IR signal, in a trade-off with spatial resolution. Increasing the force applied to a spherical tip is also expected to provide higher signal because of the resulting increase in contact area. Additionally, it is expected that all factors that influence the mechanics of tip-sample contact, such as adhesion and tip shape are expected to influence deflection and AFM-IR signal. These factors have been described by

the various quantitative treatments of contact mechanics from the AFM community [29] and will not be addressed in detail in the present work.

While the geometry of the tip-sample contact has direct bearing on the mechanics of the expansion, it can also play a role in the thermal relaxation of the sample, acting as a channel for heat conduction. Tips with higher thermal conductivity facilitate thermalization, leading to lower δ_{\max} , and lower AFM-IR signal.

A detailed understanding of the nature of heat reservoirs and heat exchange will be relevant for the optimization of photothermal measurements in fluids, such as water. To date experiments in an aqueous environment have been analyzed only in terms of mechanical factors, such as the damping of cantilever oscillations in a fluid. A thermodynamic analysis can also guide the design of new instrumental configurations, which depart from the conventional scheme based on cantilever deflection. In a more general sense, the model presented in this work can account for the diverse facets of the photothermal micromechanical detection scheme, including optical, and thermodynamic aspects in one single description.

The conclusions from this discussion are summarized in Table I, which shows the expected effect of some parameters on the intensity of the AMF-IR signal. The entries in Table I include all the quantities used for Equations 1 – 3 and can be used both as guideline for the optimization of AMF-IR experiments and as a reference to test the model described in this work.

Table I. Effect on Sample and Probe parameters on the AFM-IR signal. K : Cantilever Force Constant. A : Tip/Sample contact surface. E, E' : Young Moduli of Sample and Tip. Thermal Expansion Coefficient of Sample. σ, σ' : Poisson Ratios of Tip and Sample. F_{set} : Force Setpoint. R, R' : Radii of Tip and Sample Surface. ΔT : Photothermal Induced Temperature Increase.

Parameter	Expected Correlation with Signal Intensity
K	-
A	+
E, E'	+
α	+
σ, σ'	-
F_{set}	+
R, R'	+
ΔT	+

Testing the Photothermal Engine Model: Impulsive Excitation

The displacement of the tip from the surface increases the complexity of the analysis for the case of impulsive excitation and limits our capability to define parameters for optimization of the signal. Upon loss of contact, photoinduced forces [30] acting between tip and sample can constrain the deflection of the cantilever, effectively decreasing the AFM-IR signal. In addition, all forces affecting the interaction between tip and sample, including Van der Waals [31], electrostatic [32], and adhesion forces [31] need to be factored in in assessing the response of the cantilever as the tip-sample distance is changed. These interactions often increase in magnitude with the surface of the tip-sample contact and can offset the performance advantage provided by a larger contact area. In the case of two-material layered cantilevers, heat transmission from the heated medium [23] or direct absorption of the excitation laser light [24] can provide additional contributions to deflection, further complicating the description. Therefore, the simple guidelines obtained for the case of gradual excitation cannot be immediately extended to the case of impulsive excitation. The multiplicity of these interactions, their overlapping contributions, and the influence of environmental factors on their magnitude (e.g., the effect of humidity on capillary and electrostatic forces) provide a future challenge for the modelling of AFM-IR signal intensity in the case of pulsed excitation.

The Photothermal Engine as an Information Producing Mechanism

The quantities that are normally used to characterize the performance of classical engines, such as total work output and efficiency, appear to have no direct bearing on the performance of the AFM-IR measurement, in the sense that they do not directly relate to the intensity of the signal. Therefore, the low values of W_{tot} and η are not detrimental factors in the performance of the photothermal measurement. The AFM-IR engine has a fundamentally different purpose than a

conventional heat engine. In contrast to a classical engine, which aims to convert heat into mechanical work, the purpose of the photothermal engine in AFM-IR is the generation of information for analytical and spectroscopic purposes. The movement of the engine in response to the presence of an absorbing sample drives the movement of the AFM laser beam on the four-quadrant detector. The movement is read out as a voltage difference, which is proportional to the amplitude of the movement and provides information on the presence or absence of the absorbing material. In this context, the mechanism demonstrated by Anderson [1] fully satisfies this condition while failing to produce any useful work. This aspect will be the subject of a future separate analysis.

Conclusions

In this work we have described the detection scheme of the AFM-IR experiment in terms of a micro-to-nanoscale engine mechanism. Most of the treatment and discussion is based on AFM-IR operation relying on gradual, modulated excitation by a continuous source, as used by Anderson in the first description of the experiment.[1] We assume that the displacement of the AFM probe is determined exclusively by photothermal expansion and proposed a thermodynamic engine cycle to describe the properties of such mechanism. Forces due to tip-sample interactions other than photothermal-generated pressure have been neglected. Based on the engine model we have provided a preliminary theoretical analysis that highlights the main quantities that can affect the performance of the engine and of the associated AFM-IR experiment. We conclude that, from the perspective of classical thermodynamics, the AFM-IR engine is greatly inefficient, as most or all of the energy provided by irradiation is absorbed and dissipated as heat. Nonetheless, we also note that thermodynamic efficiency, as measured for heat engines, is not the main performance metric for such system, which is optimized for analytical and spectroscopic applications. Therefore, from the perspective of an AFM-IR experiment, the engine can be optimized for signal generation, and we provide some practical guidelines to this purpose.

We also comment on the possibility to extend this thermodynamic analysis to the more common case of impulsive excitation. In such case, tip displacement from the sample surface introduces additional contributions from multiple interactions between tip and sample which greatly increase the complexity of the analysis and limit our capability to provide simple guidelines for signal optimization. Indeed, we propose that AFM-IR experiments with continuous and with impulsive excitation are fundamentally different, and only the former relies predominantly on a measurement of the photothermal effect, while the latter responds to a multitude of additional interactions.

The present discussion is based on classical thermodynamics and is valid as long as samples can be described by their bulk properties. This is a common regime for AFM-IR samples, which in most cases are thicker than 100 nm. However, AFM-IR experiments also extend to samples 10 nm or less in size, particularly when resonant mode excitation is used, which provides signals from samples as thin as a molecular monolayer. Such measurements straddle into the realm of single molecule physics and of quantum mechanics and need models different than the macroscopic models provided here to be described satisfactorily.

Acknowledgments

Luca Quaroni was financed by an OPUS16 grant from the National Science Centre Poland under contract 2018/31/B/NZ1/01345.

The author is grateful to Dr Kirk Michaelian, Natural Resources Canada, for discussion of the fundamental aspects of photothermal spectroscopy and to Prof. Harvey Rutt, University of Southampton, for helpful comments.

References

1. Anderson, M.S. Infrared spectroscopy with an atomic force microscope. *Appl. Spectrosc.* **2000**, *54*, 349–352.
2. Quaroni, L. Infrared microscopy in the study of cellular biochemistry. *Infrared Phys. Technol.* **2020**, *105*, 102779.
3. Quaroni, L. Understanding and Controlling Spatial Resolution, Sensitivity, and Surface Selectivity in Resonant-Mode Photothermal-Induced Resonance Spectroscopy. *Anal. Chem.* **2020**, *92*, 3544–3554.
4. Dazzi, A.; Prazeres, R.; Glotin, F.; Ortega, J.M. Local infrared microspectroscopy with subwavelength spatial resolution with an atomic force microscope tip used as a photothermal sensor. *Opt. Lett.* **2005**, *30*, 2388–2390.
5. Dazzi, A. PhotoThermal Induced Resonance. Application to Infrared Spectromicroscopy. In *Thermal Nanosystems and Nanomaterials*; Volz, S., Ed.; Springer: Berlin, 2009; pp. 469–503 ISBN 978-3642042577.
6. Dazzi, A.; Prater, C.B. AFM-IR: Technology and applications in nanoscale infrared spectroscopy and chemical imaging. *Chem. Rev.* **2017**, *117*, 5146–5173.
7. Centrone, A. Infrared Imaging and Spectroscopy Beyond the Diffraction Limit. *Annu. Rev. Anal. Chem.* **2015**, *8*, 101–126.
8. Dazzi, A.; Glotin, F.; Carminati, R. Theory of infrared nanospectroscopy by photothermal induced resonance. *J. Appl. Phys.* **2010**, *107*, 124519.
9. Lu, F.; Belkin, M.A. Infrared absorption nano-spectroscopy using sample photoexpansion induced by tunable quantum cascade lasers. *Opt. Express* **2011**, *19*, 19942–7.
10. Ramer, G.; Reisenbauer, F.; Steindl, B.; Tomischko, W.; Lendl, B. Implementation of Resonance Tracking for Assuring Reliability in Resonance Enhanced Photothermal Infrared Spectroscopy and Imaging. *Appl. Spectrosc.* **2017**, *71*, 2013–2020.
11. Kenkel, S.; Mittal, A.; Mittal, S.; Bhargava, R. Probe-Sample Interaction-Independent Atomic Force Microscopy-Infrared Spectroscopy: Toward Robust Nanoscale Compositional Mapping. *Anal. Chem.* **2018**, *90*, 8845–8855.
12. Morozovska, A.N.; Eliseev, E.A.; Borodinov, N.; Ovchinnikova, O.S.; Morozovsky, N. V.; Kalinin, S. V. Photothermoelastic contrast in nanoscale infrared spectroscopy. *Appl. Phys. Lett.* **2018**, *112*, 033105.
13. O’Callahan, B.T.; Yan, J.; Menges, F.; Muller, E.A.; Raschke, M.B. Photoinduced Tip-Sample Forces for Chemical Nanoimaging and Spectroscopy. *Nano Lett.* **2018**, *18*, 5499–5505.
14. Stern, J.E.; Terris, B.D.; Mamin, H.J.; Rugar, D. Deposition and imaging of localized charge on insulator surfaces using a force microscope. *Appl. Phys. Lett.* **1988**, *53*, 2717–2719.

15. Martin, Y.; Wickramasinghe, H.K. Magnetic imaging by “force microscopy” with 1000 Å resolution. *Appl. Phys. Lett.* **1987**, *50*, 1455–1457.
16. Mayet, C.; Dazzi, A.; Prazeres, R.; Ortega, J.-M.; Jaillard, D. In situ identification and imaging of bacterial polymer nanogranules by infrared nanospectroscopy. *Analyst* **2010**, *135*, 2540.
17. Hammiche, A.; Bozec, L.; Pollock, H.M.; German, M.; Reading, M. Progress in near-field photothermal infra-red microspectroscopy. *J. Microsc.* **2004**, *213*, 129–134.
18. Donaldson, P.M.; Kelley, C.S.; Frogley, M.D.; Filik, J.; Wehbe, K.; Cinque, G. Broadband near-field infrared spectromicroscopy using photothermal probes and synchrotron radiation. *Opt. Express* **2016**, *24*, 1852.
19. Katzenmeyer, A.M.; Holland, G.; Kjoller, K.; Centrone, A. Absorption Spectroscopy and Imaging from the Visible through Mid-Infrared with 20 nm Resolution. *Anal. Chem.* **2015**, *87*, 3154–3159.
20. Zharov, V.P.; Letokhov, V.S. *Laser Optoacoustic Spectroscopy*; Springer Berlin Heidelberg: Berlin, Heidelberg, 1986; ISBN 0-387-11795-4.
21. Garcia, R.; Herruzo, E.T. The emergence of multifrequency force microscopy. *Nat. Nanotechnol.* **2012**, *7*, 217–226.
22. Nonnenmacher, M.; Wickramasinghe, H.K. Scanning probe microscopy of thermal conductivity and subsurface properties. *Appl. Phys. Lett.* **1992**, *61*, 168–170.
23. Kim, S.; Lee, D.; Thundat, T. Photothermal Cantilever Deflection Spectroscopy. *EPJ Tech. Instrum.* **2014**, *7*.
24. Kwon, B.; Rosenberger, M.; Bhargava, R.; Cahill, D.G.; King, W.P. Dynamic thermomechanical response of bimaterial microcantilevers to periodic heating by infrared radiation. *Rev. Sci. Instrum.* **2012**, *83*, 015003.
25. Weiss, L.W.; Cho, J.H.; McNeil, K.E.; Richards, C.D.; Bahr, D.F.; Richards, R.F. Characterization of a dynamic micro heat engine with integrated thermal switch. *J. Micromechanics Microengineering* **2006**, *16*, S262–S269.
26. Lu, F.; Jin, M.; Belkin, M.A. Tip-enhanced infrared nanospectroscopy via molecular expansion force detection. *Nat. Photonics* **2014**, *8*, 307–312.
27. Quaroni, L. Imaging and spectroscopy of domains of the cellular membrane by photothermal-induced resonance. *Analyst* **2020**, *145*, 5940–5950.
28. Landau, L.D.; Lifshitz, E.M. *Theory Of Elasticity*; 2nd Editio.; Pergamom Press, Oxford, 1970;
29. Garcia, R. Nanomechanical mapping of soft materials with the atomic force microscope: Methods, theory and applications. *Chem. Soc. Rev.* **2020**, *49*, 5850–5884.
30. Nowak, D.; Morrison, W.; Wickramasinghe, H.K.; Jahng, J.; Potma, E.; Wan, L.; Ruiz, R.; Albrecht, T.R.; Schmidt, K.; Frommer, J.; et al. Nanoscale chemical imaging by photoinduced force microscopy. *Sci. Adv.* **2016**, *2*.
31. Weisenhorn, A.L.; Hansma, P.K.; Albrecht, T.R.; Quate, C.F. Forces in atomic force microscopy in air and water. *Appl. Phys. Lett.* **1989**, *54*, 2651–2653.
32. Terris, B.D.; Stern, J.E.; Rugar, D.; Mamin, H.J. Localized charge force microscopy. *J. Vac. Sci. Technol. A Vacuum, Surfaces, Film.* **1990**, *8*, 374–377.